N O T I C E

THIS DOCUMENT HAS BEEN REPRODUCED FROM MICROFICHE. ALTHOUGH IT IS RECOGNIZED THAT CERTAIN PORTIONS ARE ILLEGIBLE, IT IS BEING RELEASED IN THE INTEREST OF MAKING AVAILABLE AS MUCH INFORMATION AS POSSIBLE

NASA
Technical Memorandum 87121

USAAVSCOM
Technical Report 85-C-19

Theoretical and Experimental Comparison of Vapor Cavitation in Dynamically Loaded Journal Bearings

David E. Brewe
Propulsion Directorate
U.S. Army Aviation Research and Technology Activity (AVSCOM)
Lewis Research Center
Cleveland, Ohio

Bernard J. Hamrock
Ohio State University
Columbus, Ohio

and

Bo A. Jacobson
University of Luleå
Luleå, Sweden

Prepared for the
International Symposium on Cavitation
Sendai, Japan, April 16-19, 1986

NASA

THEORETICAL AND EXPERIMENTAL COMPARISON OF VAPOR CAVITATION IN DYNAMICALLY LOADED JOURNAL BEARINGS

David E. Brewe
Propulsion Directorate
U.S. Army Aviation Research and Technology Activity (AVSCOM)
Lewis Research Center
Cleveland, Ohio 44135

Bernard J. Hamrock
Ohio State University
Columbus, Ohio 43210

and

Bo O. Jacobson
University of Lulea
Lulea, Sweden

SUMMARY

An experimental and theoretical investigation of vapor cavitation is made for a submerged journal bearing under dynamically loaded conditions. The observance of vapor cavitation in the laboratory was made possible using high-speed photography. Vapor cavitation was found to occur when the tensile stress applied to the oil exceeded the tensile strength of the oil or the binding of the oil to the surface. The theoretical solution to the Reynolds equation is determined numerically using a moving boundary algorithm. This algorithm conserves mass throughout the computational domain including the region of cavitation and its boundaries. An ADI (Alternating Direction Implicit) method is used to effect the time march. A study of a rotor undergoing circular whirl was conducted. Predicted cavitation behavior was analyzed using three-dimensional computer graphic movies. The formation, growth, and collapse of the bubble in response to the dynamic conditions is shown. For the same conditions of dynamic loading, the cavitation bubble was studied in the laboratory using high-speed photography. Movies comparing experiment with theory will be presented.

E-2729

INTRODUCTION

The most common cavitation boundary condition for steadily loaded bearings is the zero-pressure-gradient condition of Swift and Stieber (refs. 1 and 2). This condition results from the assumption of continuity of mass flow at the boundary between the cavitation zone and the liquid-filled regions under steady state conditions. In many bearings, however, dynamic loads cause changes in the local film thickness, and the problem of determining the appropriate boundary condition requires a condition other than zero pressure gradient at the boundary. The studies of Olsson (refs. 3 and 4) suggest that the usual steady state condition, $p = dp/dx = 0$, is adequate for dynamic situations if the cavitation boundary moves at a speed that is less than half the journal surface speed. However, if the cavitation boundary moves at a speed that is greater than half the journal surface speed, a more realistic formulation of the boundary condition should be developed.

Jakobsson-Floberg (ref. 5) and Olsson (ref. 3) formulated boundary conditions for a moving boundary that conserved mass within the cavitated region as well as at the boundary (commonly referred to as the JFO cavitation theory). It was assumed that liquid was convected through the cavitated region in the form of striations extending to both surfaces in the film gap. The striated flow in the JFO theory is necessarily a Couette flow because of a constant pressure assumption within the cavitated region. Jakobsson and Floberg's experimental findings (ref. 5) support the constant pressure assumption. The JFO theory perhaps represents one of the best accounts of a dynamical theory to date for moderately to heavily loaded journal bearings and/or dampers. It is an improvement over the Swift-Stieber conditions, even for steady-state solutions, because it provides for film reformation or fillback as well as film rupture. Both rupture and fillback require a knowledge of the pressure gradient and fractional film content at the interface to determine its location. Unlike a rupture boundary, the fillback boundary is subjected to a pressure flow (i.e., nonzero pressure gradient). Further, the fractional film content at the boundary is determined by a residual fluid within the cavitated region that has been released at a rupture boundary (earlier in time) and governed by the fluid transport law. Which condition (fillback or rupture) prevails, depends upon the relative motion of the boundary with the motion of the convected fluid normal to the boundary. Typically, under steady-state cavitating conditions, the rupture boundary occurs along the upstream boundary and the fillback boundary occurs along the downstream end. Under dynamic loading and nonstationary cavitation, rupture or fillback conditions may be required at either the upstream or the downstream boundary. To effect these conditions in a computational algorithm, the programming task is exceedingly tedious and this discourages their implementation in current practice.

Elrod and Adams (ref. 6) introduced a computational scheme that mimics the JFO theory. It avoids the complex programming required to trace the moving boundary between grid points and evaluating the required pressure derivative. Later, Elrod (ref. 7) modified it and presented it in more detail. The algorithm incorporates a switching function that "switches out" any pressure flow within the cavitated region. This automatically introduces a cavity conforming to the requirements of mass continuity and the JFO theory. Elrod has compared results generated by the algorithm with experimental results of Lundholm (ref. 8) for steady-state operation of a circumferentially fed journal bearing. The results (i.e., cavitation extent, load capacity, and attitude-angle versus eccentricity) were quite good. For steady-state applications, Lebeck et al. (ref. 9) and Miranda (ref. 10) have used the Elrod algorithm. Brewe (ref. 11) was one of the first to apply the algorithm to a submerged journal bearing operating under dynamically loaded conditions. The solution to the Reynolds equation is determined numerically using a control volume method. This method conserves mass throughout the computational domain including the liquid-vapor interface which may or may not be in motion relative to the minimum film line. An ADI (Alternating Direction Implicit) method is used to effect the time march.

To the authors knowledge, Jacobson and Hamrock (ref. 12) was the first paper to experimentally illustrate the development of vapor cavitation in a dynamically loaded journal bearing. A high-speed motion picture camera was used to capture the formation and collapse of the vapor bubble in the journal bearing.

The theoretical formulation presented by Brewe (ref. 11) will be used to describe the formation, growth, and collapse of a vapor cavitation bubble in response to conditions in a dynamically loaded journal bearing. For the same conditions of dynamic loading, the cavitation bubble will be studied using the experimental apparatus of Jacobson and Hamrock (ref. 13). The development of the vapor cavitation will be shown using the high-speed photography and these results will be directly compared with the computer simulated results.

SYMBOLS

D	shaft diameter, m
e	eccentricity, m
g	switch function (cavitation index)
h	film thickness, m
L/D	length to diameter ratio
$\dot{m}_x$, $\dot{m}_z$	lineal mass flux, kg/ms
p	fluid pressure, N/m^2
p_a	ambient pressure, N/m^2
p_c	cavitation pressure, N/m^2
R	radius of shaft, m
ΔR	radial clearance, m
t	time, s
U	sum of the surface velocities in x-direction, m/s
w	squeeze-velocity, m/s
x	coordinate along circumference, m
Δx	incremental spacing along circumference, m
y	coordinate normal to x, z-plane, m
z	axial coordinate, m
Δz	axial incremental spacing, m
β	liquid bulk modulus, N/m^2
γ	angular position of minimum film, rad

ϵ eccentricity ratio, $e/\Delta R$

θ fractional film content in cavitation zone, density ratio (ρ/ρ_C) in full film zone

μ dynamic viscosity, Ns/m

ρ_C fluid density within cavitated zone, kg/m

φ angular coordinate relative to minimum film line, rad

ω_d orbital angular velocity of journal center about fixed point relative to the housing center, rad/s

ω_s angular velocity of journal about its own center, rad/s

Subscripts:

d dynamic

s static

APPARATUS AND TEST PROCEDURE

The experimental setup with the high-speed camera, motors, and test rig is shown in figure 1. The high-speed motion picture camera that was used could take up to 11 000 frames/sec with ordinary 16-mm motion picture film. In the experiments presented in this report the framing rate was 2000 frames/sec.

The test bearing was lubricated by gravity feed from a can placed approximately 600 mm above the bearing. The test lubricant was a nondegassed Dexron-II type of automatic transmission fluid with a viscosity of 0.066 N s/m at atmospheric conditions. The lubricant passed from the can through a line and entered the bearing at the top left of the polymethylmethacrylate (PMMA) bearing shown in figure 1. At the right in figure 1 is the motor that gives the sliding velocity to the roller, and at the left is the motor that gives the squeeze velocity to the bearing. The speeds of these identical 0.5-kW motors can vary continuously from 0 to 250 rad/s.

Figure 2 shows the PMMA bearing, which can vibrate in a circular motion keeping the axis of vibration parallel to the axis of rotation. The special mechanism manufactured to keep the centerline of the bearing parallel to the centerline of the journal when the bearing is vibrating is shown in figure 2. It consists of three plates each coupled together with four thin plates made from spring steel. The spring steel plates could easily be bent in the direction perpendicular to the plates but were very stiff in the horizontal planes of the plates. Because of the symmetry of the mechanism the thick plates were always parallel to each other when the thin plates were bent as long as they did not buckle.

The dynamic eccentricity mechanism shown assembled in figure 2 enables one to vary the dynamic eccentricity from 0 to 0.5 mm. Since the radial clearance is 0.5 mm, the ratio of the dynamic eccentricity to the radial clearance can be varied between 0 and 1. The amplitude of the vibration of the squeeze motion is given by the dynamic eccentricity ratio. By setting the dynamic eccentricity equal to zero and moving the journal relative to the centerline of the bearing, the static eccentricity can be varied between 0 and 0.5 mm, meaning that the static eccentricity ratio can be varied between 0 and 1. Therefore the offset of the center of vibration from the center of the journal gives a static load, and the amplitude of the vibration gives a variable rotating dynamic load superimposed on the static load. Both the location of the center of vibration and the amplitude of vibration can vary.

Figure 3 shows four positions of the journal relative to the bearing for a dynamically loaded journal bearing. The static eccentricity ratio ϵ_s is set at 0.34, and the dynamic eccentricity ratio ϵ_d is set at 0.66. The direction of the dynamic eccentricity rotates 90° counterclockwise going from (a) to (b), (b) to (c), and (c) to (d). In figure 3 the squeeze and separation component of motion is clearly visible.

EXPERIMENTAL RESULTS

Figure 4 presents several frames from the high-speed films showing the formation and collapse of vapor cavitation in a journal bearing. The actual film provides a better illustration; however, the figures highlight the film. The fixed conditions for figure 4 are $L/D = 1/4$, $\epsilon_s = 0.340$, $\epsilon_d = 0.660$, $0.32 \leq \epsilon \leq 1.0$, $\omega_s = 19.5$ rad/s, $\omega_d = 92.7$ rad/s, and PTFE journal surface. The framing rate of the camera was 2000 frames/s. The time from the first frame to the last in figure 4 was less than 25 ms, indicating how rapidly the vapor cavitation forms and collapses.

The sample frames filmed (fig. 4) illustrate that in dynamically loaded journal bearings cavitation bubbles containing mainly oil vapor are present. Vapor cavitation occurred when the tensile stress applied to the oil exceeded the tensile strength of the oil or the binding of the oil to the surface. To the author's knowledge, other than our initial report (ref. 3), this was never shown before. Vapor cavitation is quite different from gas cavitation. The gas cavitation bubbles can be transported through the high-pressure region of the bearing as demonstrated in Jacobson and Hamrock (ref. 13). On the other hand, vapor cavitation bubbles dissolve and disappear in less than a hundredth of a cycle of vibration. Without a high-speed camera one would not be able to observe vapor cavitation. Furthermore, this type of cavitation can cause erosive wear (ref. 14) of adjacent surfaces, so its presence in dynamically loaded journal bearings is an important observation.

THEORETICAL MODEL

Elrod and Adams (ref. 6) implemented a moving boundary scheme that avoids interface complications. The following reveals some of the underlying factors that led up to the algorithm which was later modified by Elrod (ref. 7) and used here. The conservation of mass can be written in the following way:

$$\frac{\partial(\rho h)}{\partial t} + \vec{\nabla} \cdot \vec{m} = 0 \qquad (1)$$

where $\dot{\vec{m}}$ represents the lineal mass flux and is given by

$$\dot{\vec{m}} = \rho \frac{h\vec{V}}{2} - \frac{\rho h^3}{12\mu} \vec{\nabla} p \tag{2}$$

Substitution of equation (2) into (1) leads to the Reynold's lubrication equation. This equation has been made applicable to the cavitation region as well as the full film region by incorporating a switch function to automatically satisfy the boundary conditions at a moving interface. Further, the fractional film content, θ, has been made the dependent variable. This required giving θ a dual interpretation. That is, in the full film region, θ represents the mass content of the film that exceeds the content that would exist if the pressure were at cavitation pressure, p_c. In other words,

$$\theta = \rho/\rho_c \tag{3}$$

where ρ_c is the density of the liquid at the pressure p_c. Further, p and θ are related through the equation for the liquid bulk modulus according to

$$\rho \frac{\partial p}{\partial \rho} = \beta \tag{4}$$

or

$$p = p_c + \beta \ln \theta \qquad \theta \geq 1.0 \tag{5}$$

In the cavitation region ($\theta < 1.0$) determines the mass content ($\rho_c \theta h$) which can manifest itself in the form of a smeared mass or striated flow extending to both surfaces in the film gap. The fluid transported through the cavitation region in the form of an adhered film can be neglected for heavily loaded conditions.

Having linked the solutions of the full film region with the solutions in the cavitated region via a single dependent variable, θ, a universal differential equation is made possible. However, a cavitation index, or switch function, g, was introduced so that the resulting PDE would be consistent with the uniform pressure assumption within the cavitated region. The switch function is defined from a knowledge of θ. Thus

$$\begin{aligned} g &= 0; \qquad \theta \quad 1.0 \\ g &= 1; \qquad \theta \quad 1.0 \end{aligned} \tag{6}$$

and g is made a factor of the pressure gradient term in equation (2) so that the flow is strictly Couette in the cavitated region. Expressing the lineal mass flux, $\dot{\vec{m}}$, in terms of θ, and g and substituting into equation (1) results in the universal differential equation obtained in Elrod and Adams (ref. 6); i.e.,

$$\frac{\partial(\theta\vec{h})}{\partial t} + \frac{\vec{V}}{2} \cdot \vec{\nabla}(\theta h) = \vec{\nabla} \cdot \frac{h}{12\mu} \beta g(\theta) \vec{\nabla}\theta \tag{7}$$

In the full film region the solutions of θ together with equation (5) determine the pressures. In the cavitation region, $g = 0$, and equation (7) becomes

$$\frac{\partial(\theta h)}{\partial t} + \frac{\vec{V}}{2} \cdot \vec{\nabla}(\theta h) = 0 \tag{8}$$

governing the transport of the fluid through the cavitation region.

Making use of information from Brewe (ref. 11) the resulting convective and pressure flow equations can be expressed as

$$(\Delta m_x)_{conv} = \frac{\rho_c U}{2}\left[h_{-1}(1 - g_{-1})\theta_{-1} - h_0(1 - g_0)\theta_0 + \frac{g_{-1}h_{-1}}{2}(2 - g_0) + \frac{g_0 h_0}{2}(g_{-1} - 2 + g_1) + \frac{g_1 h_1 g_0}{2}\right] \tag{9}$$

$$(\Delta \dot{m}_x)_{press} = \frac{\rho_c \beta}{12\mu}\left[\frac{h^3_{-1/2} g_{-1}(\theta_{-1} - 1) - (h^3_{-1/2} + h^3_{+1/2}) g_0(\theta_0 - 1)}{\Delta x} + \frac{h^3_{+1/2} g_1(\theta_1 - 1)}{\Delta x}\right] \tag{10}$$

In this study, an alternating direction implicit (ADI) scheme was applied. The implicit Euler method was used to advance the time at each half time step since this is known to be unconditionally stable (ref. 15) insofar as the ordinary differential equation is stable. In the first half time step, a differencing along the circumference is performed that leads to a system of equations that can be expressed using a periodic tridiagonal matrix. The solutions of θ along the circumference are found by performing a Gauss-Jordan reduction on the periodic matrix using a maximum-pivot strategy to reduce the error. In the second half time step differencing along the axial direction leads to a system of equations that can be expressed in pure tridiagonal form. These solutions are readily obtained by using a nonpivoted Gaussian elimination procedure (tridiagonal solver). Since the journal and housing are aligned, the pressures must be symmetric about the axial center. Consequently, the calculations are only made over half the axial length of the housing.

The switch function was updated after each half-time step. Occasionally, during the collapse of the vapor bubble, liquid was piling up at the boundary. It appears that the switch function was not accommodating the movement of the boundary adequately for that time step (private communication, H.G. Elrod). Consequently, the switch function was immediately updated and the calculation was reiterated.

THEORETICAL RESULTS

A numerical scheme (ref. 11) based upon the Elrod algorithm was devised to study vapor cavitation in a submerged journal bearing for both steady and dynamic loading. The method conserves mass throughout the computational domain including the region of cavitation. In this investigation, the algorithm was checked against experimental data for a journal whirling in a circular path through one orbit.

Figure 5 illustrates the bearing configuration along with the predicted pressure distribution that resulted from Brewe's (ref. 11) numerical calculations using the Elrod algorithm. The journal is rotating in a counter clockwise direction. Thus, the entrainment velocity through the minimum film is in a counter clockwise direction, and by convention considered positive. The line of centers extends through the position of minimum film thickness. The positive pressures seen in the three-dimensional plot of figure 5 are generated in the converging clearance region adjacent to this line. In the direction of rotation, the pressures become subambient in the diverging clearance region. The upstream and downstream meniscus of the cavitation boundary is outlined there. The corresponding extent of cavitation is shown by the dark shaded area in the three-dimensional plot. Figure 5 illustrates the similarities and differences of the pressure distribution as they occur throughout the entire orbit. Frame (a) represents the position of the journal within the housing and the associated pressure distribution at the initial instant in time. The pressure buildup due to the combined squeezing and sliding motion of the journal is shown for the first half cycle in frames (a) through (d). It should be noted in comparing frames (c) and (d), that the maximum peak pressure does not occur when the eccentricity is a maximum as one might first expect. This can be explained by referring to figure 6 and noting that the squeeze velocity approaches zero and the sliding velocity approaches a minimum at the end of the half cycle. This offsets the effectiveness of generating increasing pressures due to a decreasing film. The onset of cavitation occurs at frames (b) 25 ms into the cycle. The squeeze component is known to suppress the conditions for cavitation (ref. 16). Proceeding from (d) to (e), shows the journal (near the minimum film line) is separating from the bearing. The initial stages of separation creates a suction effect, causing the pressure hump to dissipate and the vapor bubble to expand. Note that frames (b) and (e) were both generated at the same value of eccentricity. The essential difference is that the squeeze velocity has a different sign. That is, when the squeeze velocity is negative (i.e., the clearance is decreasing), the motion of the journal is producing a squeeze effect (frame b). In frame (e), the squeeze velocity is positive (i.e, the clearance is increasing) and produces a suction. Here the vapor bubble has actually crossed the minimum film line and been drawn into the converging clearance space of the bearing. As the journal continues to pull away from the bearing, the increased clearance means that a much greater Poiseuille side flow is present to cause the collapse of the bubble. This is because the Poiseuille side flow is proportional to h^3. In frame (f), the bubble has drifted downstream from the minimum film line and is collapsing.

COMPARISON OF EXPERIMENTAL AND THEORETICAL RESULTS

The formation, growth, and collapse of the bubble in response to dynamic conditions is compared experimentally and theoretically. High-speed photography revealed in figure 4 that for the conditions listed previously, the

vapor bubble remained visible for a period of at least 23 ms. This represented approximately one-third of the full dynamic cycle of the bearing.

The predicted life of the vapor bubble shown in figure 5 from the computer code was 32 ms. A part of this difference arises because this measure of bubble life inherently contains a certain duration of time for which the computer indicates cavitation although in reality it would be invisible to the eye. This is probably not the major contributing factor to the discrepancy, however. The pressures calculated for these conditions were of the order of 10^7 N/m^2. A plastic (polymethylmethacrylate, PMMA) was used as a housing material for viewing purposes. It is thus most likely that deformation and temperature effects in the experiments are responsible for the discrepancy, not accounted for by the numerical method. Further, the experiment allowed the eccentricity to reach a maximum value of 1.0, whereas a certain amount of numerical instability was observed when the eccentricity exceeded 0.98. Consequently, the input conditions for the computations were not identical to the input conditions of the experiment.

CONCLUSIONS

A theoretical and experimental investigation is made of the evolution of a vapor-bubble for a submerged journal bearing under dynamically loaded conditions. The theoretical solution to the Reynolds equation is determined numerically using a control volume method (Elrod algorithm). This method conserves mass throughout the computational domain including the liquid-vapor interface which may or may not be in motion relative to the minimum film line. An ADI method is used to effect the time march.

The occurrence of vapor cavitation was clearly evident in both the theoretical as well as the experimental results presented. Vapor cavitation occurred when the tensile stress applied to the oil exceeded the tensile strength of the oil or the binding of the oil to the surface. The physical situation causing the vapor cavitation was a squeezing and sliding motion within a bearing. Good agreement was found between theory and experiment. A prediction of 32 ms bubble life for nonstationary cavitation was obtained from the dynamic theory. Using high-speed photography for the same set of conditions, a bubble life of 23 ms was observed in the laboratory. This discrepancy was attributed to deformation and temperature effects as well as some uncertainty in correlating actual life with duration of visibility. Furthermore, the maximum eccentricity in the experiments was 1.0. Numerical instabilities prohibited eccentricities larger than 0.98.

REFERENCES

1. Swift, H.W., "The Stability of Lubricating Films in Journal Bearings," Proceedings of the Institution of Civil Engineers, Vol. 23, No. 4809, 1932, pp. 267-288, Discussion pp. 289-322.

2. Stieber, W., "Das Schwimmlager, Hydrodynamische Theorie des Gleitlagers," VDI-Verlag, Berlin, 1933.

3. Olsson, K.O., "Cavitation in Dynamically Loaded Bearings," Chalmers University of Technology, Goteborg, 1965.

4. Olsson, K.O., "On Hydrodynamic Lubrication with Special Reference to Non-stationary Cavitation," Chalmers University of Technology, Goteborg, 1974.

5. Jakobsson, B., and Floberg, L., "The Finite Journal Bearing Considering Vaporization," Chalmers Tekniska Hoegskolas Handlingar, Vol. 190, 1957, pp. 1-116.

6. Elrod, H.G., and Adams, M.L, "A Computer Program for Cavitation and Starvation Problems," in, Cavitation and Related Phenomena in Lubrication. Mechanical Engineering Publications, New York, 1974, pp. 37-41.

7. Elrod, H.G., "A Cavitation Algorithm," Journal of Lubrication Technology, Vol. 103, No. 3, July 1981, pp. 350-354.

8. Lundholm, G., "The Circumferential Groove Journal Bearing Considering Cavitation and Dynamic Stability," Acta Polytechnica Scandinavica, Mechanical Engineering Series, No. 42, 1969, pp. 1-89.

9. Lebeck, A.O., Teale, J.L., and Pierce, R.E., "Hydrodynamic Lubrication with Wear and Asperity Contact in Mechanical Face Seals," Annual Report ME-86(78)Onr-414-1, Bureau of Engineering Research, The University of New Mexico, Albuquerque, N.M., Jan. 1978. (AD-A050783)

10. Miranda, A.A.S., "Oil Flow, Cavitation and Film Reformation in Journal Bearings Including an Interactive Computer-Aided Design Study," Ph.D. Thesis, Univ. of Leeds, U.K., 1983.

11. Brewe, D.E., "Theoretical Modeling of the Vapor Cavitation in Dynamically Loaded Journal Bearings," NASA TM-87076, National Aeronautics and Space Administration, 1985.

12. Jacobson, B.O., and Hamrock, B.J., "High-Speed Motion Picture Camera Experiments of Cavitation in Dynamically Loaded Journal Bearings," Journal of Lubrication Technology, Vol. 105, No. 3, July 1983, pp. 446-452.

13. Jacobson, B.O. and Hamrock, B.J., "Vapor Cavitation in Dynamically Loaded Journal Bearings," NASA TM-83366, National Aeronautics and Space Administration, 1983.

14. Wilson, R.W., "Cavitation Damage in Plain Bearings," in Cavitation and Related Phenomena in Lubrication. Mechnical Engineering Publications, New York, 1974, pp. 177-184.

15. Warming, R.F., and Beam, R.M., "An Extension of A-Stability to Alternating Direction Implicit Methods," NASA TM-78537, National Aeronautics and Space Administration, 1978.

16. Ghosh, M.K., Hamrock, B.J., and Brewe, D.E., "Hydrodynamic Lubrication of Rigid Nonconformal Contacts in Combined Rolling and Normal Motion," Journal of Tribology, Vol. 107, No. 1, Jan. 1985, pp. 97-103.

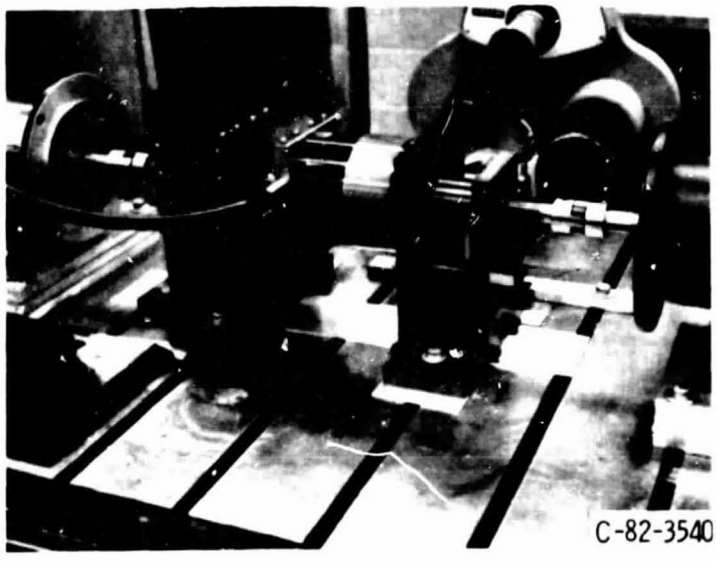

Figure 1. - Test apparatus.

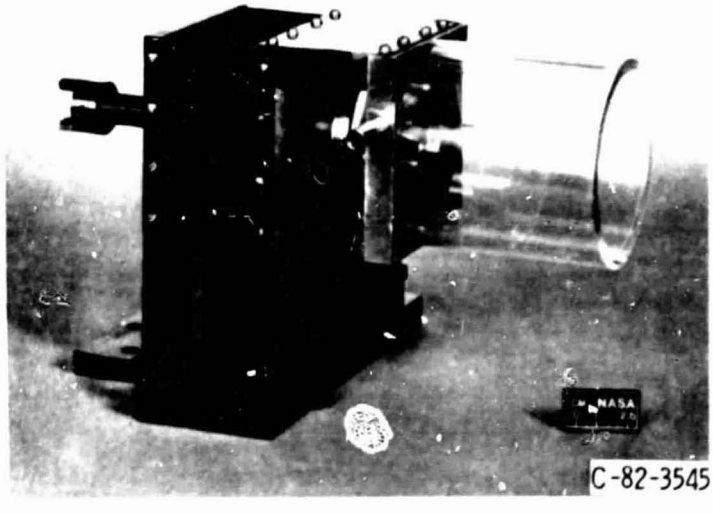

Figure 2. - PMMA-tube and eccentric.

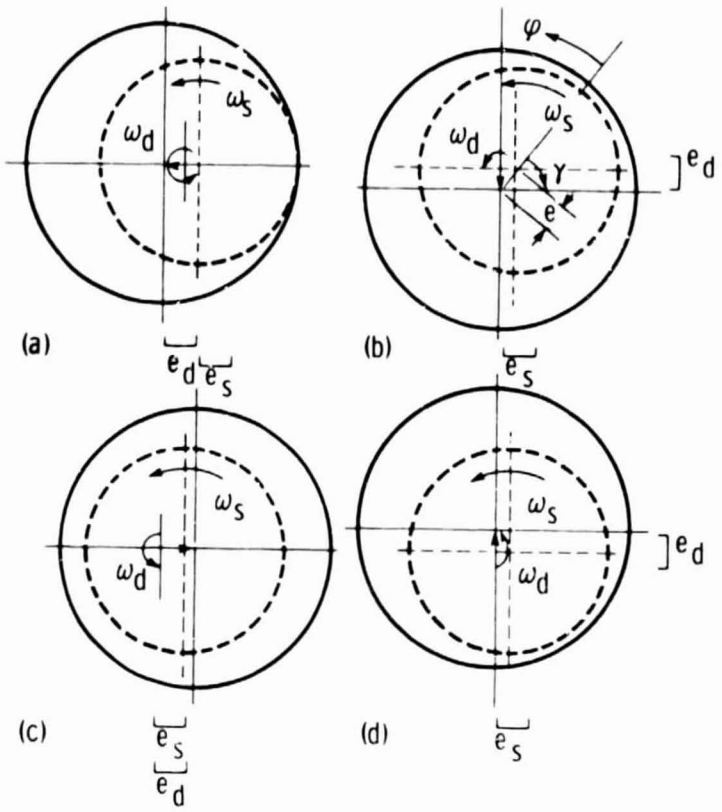

Figure 3. - Bearing geometries at four different times.

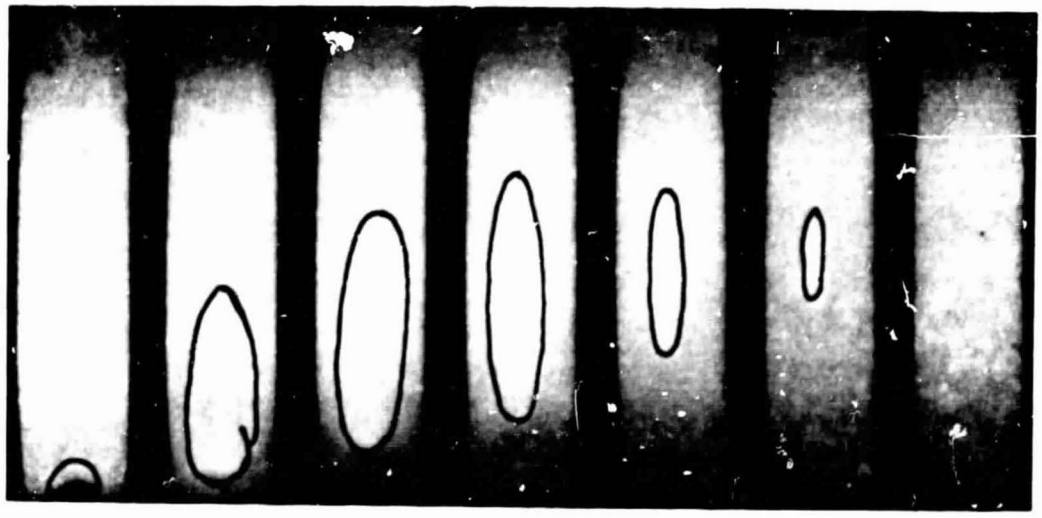

(a) t = 4 ms (b) t = 12 ms (c) t = 18 ms (d) t = 20 ms (e) t = 23 ms (f) t = 24 ms (g) t = 25 ms

Figure 4. - Intermittent stages of non-stationary cavitation using high-speed photography.

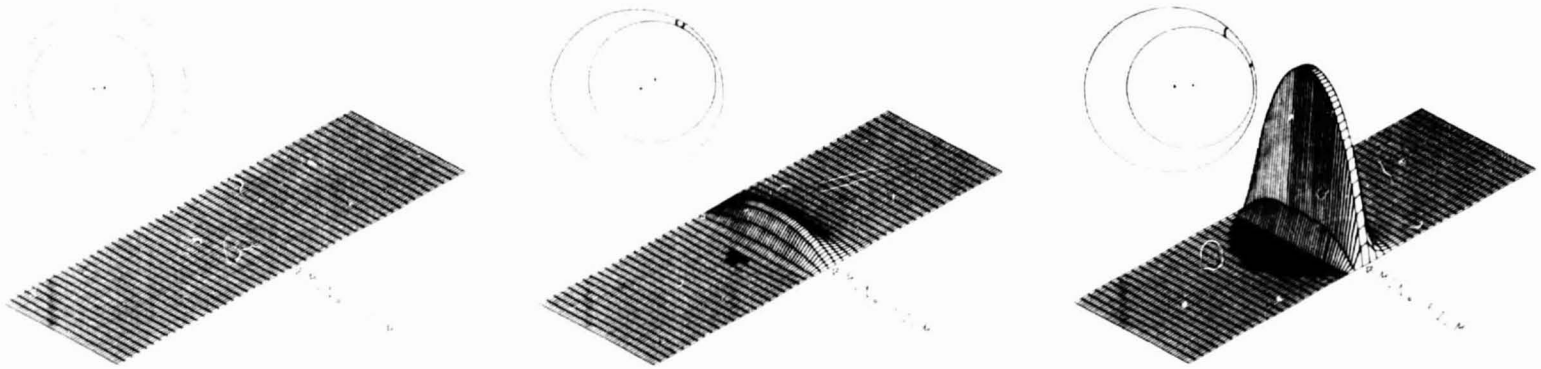

(a) Initial conditions (t = 0; e = 0.32).

(b) Squeeze motion (t = 25 ^ ms: e = 0.91).

(c) Occurance of peak load (t = 32.2 ms: e = 0.977).

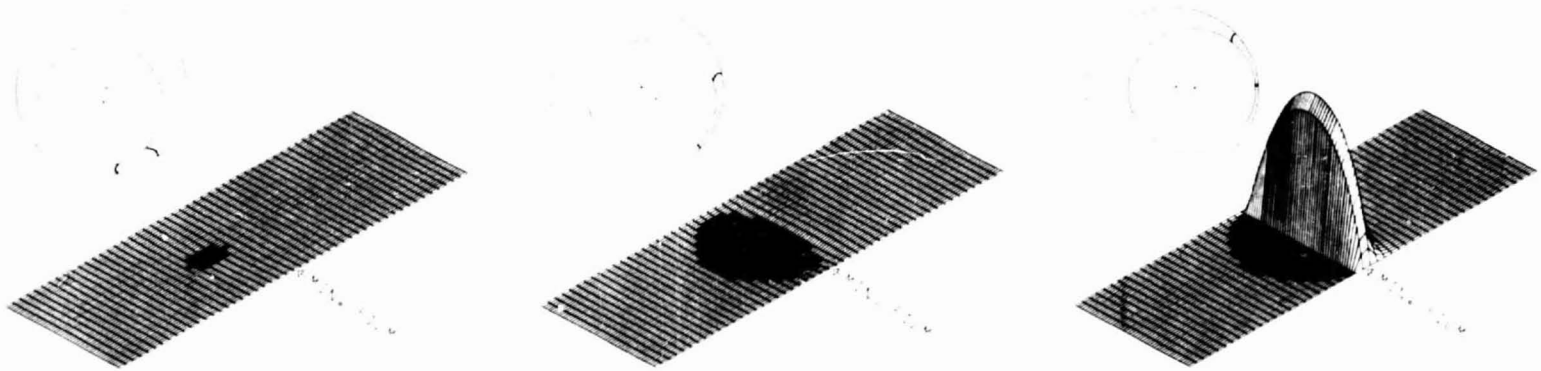

(f) Bubble collapse (t = 56.1 ms: e = 0.57).

(e) Bubble expands (t = 42.6 ms: e = 0.91).

(d) Begin separation (t = 33.9 ms: e = 0.980).

Figure 5. - Pressure distribution and bearing configuration for a full period of shaft whirl, using Elrod's algorithm. The figures (a-f) viewed in clockwise order are consecutive in time.

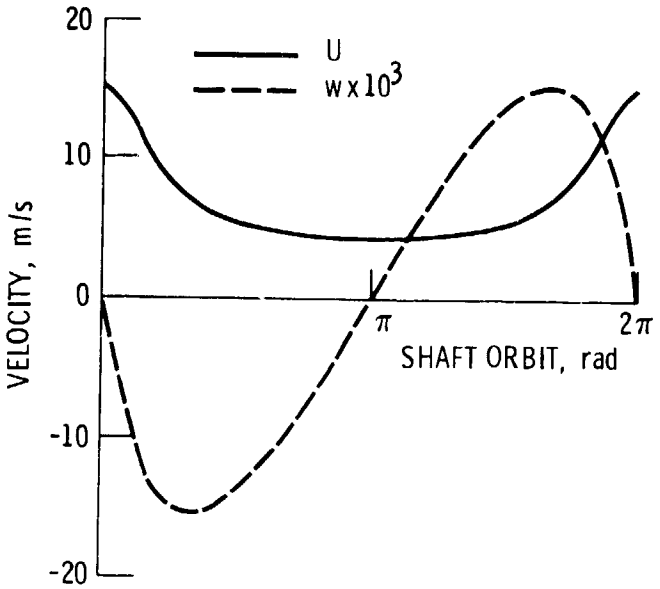

Figure 6. - Surface velocity sum (U) and squeeze velocity (w) during a full period of shaft whirl.

1. Report No. NASA TM-87121 USAAVSCOM-TR-85-C-19	2. Government Accession No.	3. Recipient's Catalog No.

4. Title and Subtitle	5. Report Date
Theoretical and Experimental Comparison of Vapor Cavitation in Dynamically Loaded Journal Bearings	6. Performing Organization Code 505-33-62
7. Author(s) David E. Brewe, Bernard J. Hamrock, and Bo O. Jacobson	8. Performing Organization Report No E-2729
	10. Work Unit No.
9. Performing Organization Name and Address NASA Lewis Research Center and Propulsion Directorate U.S. Army Aviation Research and Technology Activity (AVSCOM), Cleveland, Ohio 44135	11. Contract or Grant No.
	13. Type of Report and Period Covered Technical Memorandum
12. Sponsoring Agency Name and Address National Aeronautics and Space Administration Washington, D.C. 20546 and U.S. Army Aviation Systems Command, St. Louis, Mo. 63120	14. Sponsoring Agency Code

15. Supplementary Notes

David E. Brewe, Propulsion Directorate, U.S. Army Aviation Research and Technology Activity (AVSCOM), Lewis Research Center, Cleveland, Ohio; Bernard J. Hamrock, Ohio State University, Columbus, Ohio 43210; Bo O. Jacobson, University of Luleå, Luleå, Sweden. Prepared for the International Symposium on Cavitation, Sendai, Japan, April 16-19, 1986.

16. Abstract

An experimental and theoretical investigation of vapor cavitation is made for a submerged journal bearing under dynamically loaded conditions. The observance of vapor cavitation in the laboratory was made possible using high-speed photography. Vapor cavitation was found to occur when the tensile stress applied to the oil exceeded the tensile strength of the oil or the binding of the oil to the surface. The theoretical solution to the Reynolds equation is determined numerically using a moving boundary algorithm. This algorithm conserves mass throughout the computational domain including the region of cavitation and its boundaries. An ADI (Alternating Direction Implicit) method is used to effect the time march. A study of a rotor undergoing circular whirl was conducted. Predicted cavitation behavior was analyzed using three-dimensional computer graphic movies. The formation, growth, and collapse of the bubble in response to the dynamic conditions is shown. For the same conditions of dynamic loading, the cavitation bubble was studied in the laboratory using high-speed photography. Movies comparing experiment with theory will be presented.

17. Key Words (Suggested by Author(s))	18. Distribution Statement
Cavitation; Hydrodynamics; Journal bearing; Vapor caviation; High-speed photography	Unclassified - unlimited STAR Category 34

19. Security Classif. (of this report)	20. Security Classif. (of this page)	21. No. of pages	22. Price*
Unclassified	Unclassified		

*For sale by the National Technical Information Service, Springfield, Virginia 22161